Earth and Space Science

RESEARCH LETTER
10.1029/2024EA003854

Hollows on Mercury: A Comprehensive Analysis of Spatial Patterns and Their Relationship to Craters and Structures

Barbara De Toffoli[1,2], Valentina Galluzzi[1], Matteo Massironi[2], Sebastien Besse[3], Gene Walter Schmidt[1], Oceane Barraud[4], Salvatore Buoninfante[1,5], and Pasquale Palumbo[1]

[1]INAF, Istituto di Astrofisica e Planetologia Spaziali, Rome, Italy, [2]Department of Geosciences, Università Degli Studi di Padova, Padova, Italy, [3]European Space Agency (ESA), European Space Astronomy Centre (ESAC), Madrid, Spain, [4]Institute for Planetary Research, DLR, Berlin, Germany, [5]Department of Earth, Environment and Resources Sciences (DiSTAR), Università Degli Studi di Napoli Federico II, Naples, Italy

Key Points:

- We renewed the global database of hollow fields adding 41 new observations for a total of 476
- Hollows formation is not linked to a singular widespread source layer due to a lack of correlation with specific units or depth ranges
- Hollows are short-lived features which preferentially form in fresh craters or older craters that are disturbed by reworking

Supporting Information:

Supporting Information may be found in the online version of this article.

Correspondence to:

B. De Toffoli,
barbara.detoffoli@inaf.it;
barbara.detoffoli@unipd.it

Citation:

De Toffoli, B., Galluzzi, V., Massironi, M., Besse, S., Schmidt, G. W., Barraud, O., et al. (2024). Hollows on Mercury: A comprehensive analysis of spatial patterns and their relationship to craters and structures. *Earth and Space Science*, *11*, e2024EA003854. https://doi.org/10.1029/2024EA003854

Received 4 JUL 2024
Accepted 17 OCT 2024

Author Contributions:

Conceptualization: Barbara De Toffoli, Valentina Galluzzi, Matteo Massironi
Data curation: Barbara De Toffoli
Formal analysis: Barbara De Toffoli
Funding acquisition: Pasquale Palumbo
Investigation: Barbara De Toffoli
Methodology: Barbara De Toffoli
Project administration: Valentina Galluzzi, Pasquale Palumbo
Supervision: Valentina Galluzzi, Pasquale Palumbo
Visualization: Barbara De Toffoli
Writing – original draft: Barbara De Toffoli, Valentina Galluzzi
Writing – review & editing: Matteo Massironi, Sebastien Besse, Gene

Abstract Hollows on Mercury are small (hundreds of meters - few kilometers), shallow (tens of meters), irregular depressions typically found in clusters, often associated with impact craters, and likely formed by the loss of volatile materials. While their exact formation process remains debated, various hypotheses suggest sublimation or space weathering. In this study, we analyzed the global distribution of hollows, exploring their spatial patterns and relationships with key geological features. Our findings challenge the idea that hollows arise from a single volatile-rich surface layer, suggesting instead that volatiles are dispersed throughout the crust. Hollows show no correlation with specific geological units or elevations, indicating no singular volatile source. Moreover, the transitory nature of hollows is suggested as they are rare in older, degraded craters but common in younger ones or older craters with deep-seated features, hinting at a link to the reworking of materials through impacts or volcano-tectonic activity.

Plain Language Summary Mercury's surface is widely covered with hollows, that is, small, localized, shallow depressions found on the surface of the planet and often linked to impact craters. We studied the global distribution of hollows and connections with other geological features. We found no evidence for a single layer of volatile materials driving their formation and instead volatiles seem to be scattered throughout the entirety of the exposed crust. Hollows do not seem to have strong ties to specific geological formations or elevation ranges, indicating a complex and/or non unified origin. They also seem to form and disappear quickly, being rare or absent in older, worn-down craters compared to younger ones. Interestingly, they are more common in fresh craters or older ones with younger pits and tectonic features which suggests that they form when existing materials are disturbed by impacts or volcanic and tectonic activity. This suggests a dynamic relationship between Mercury's surface processes and the formation of these intriguing features.

1. Introduction

Mercury's hollows are small (hundreds of meters to a few kilometers in diameter), localized, shallow (tens of meters) depressions found on the surface of the planet. They are unique features distinct from their surroundings, and characterized by their appearance as irregular, bright spots, often found clustered in groups called hollow fields. The distribution of hollows is characterized by a widespread, but non-uniform spatial pattern (Blewett et al., 2011). Images captured by MESSENGER (MErcury Surface, Space ENvironment, GEochemistry, and Ranging; Solomon et al., 2007) have revealed the morphological diversity of these hollows, ranging from irregularly shaped depressions with scalloped edges to smoother, flat-floored structures (Blewett et al., 2013). Hollows are present in most types of terrains, particularly craters, and cover a wide range of latitudes including the Low Reflectance Materials (LRM) regions (Thomas et al., 2014a). Notably, hollows consistently appear morphologically (sharp) and spectrally (bright and less red - increasing reflectance with increasing wavelength) fresh, and lack superposed impact craters which indicates a relatively recent formation (Blewett et al., 2011; Murchie et al., 2015).

Since their discovery with MESSENGER (Blewett et al., 2011), hollows have been extensively observed and analyzed, progressively increasing our understanding of them. Their origin is still not fully understood, but they are believed to be related to space-weathering processes (e.g., micrometeoroid impacts; solar wind; charged particles bombardment processes) or sublimation processes, where volatile materials (Barraud et al., 2020, 2023; Blewett et al., 2013) directly transition from solid to gas due to exposure to high temperatures induced, for

Walter Schmidt, Oceane Barraud, Salvatore Buoninfante

example, by intense sunlight or volcanic activity (Blewett et al., 2011), or as part of volatile degassing produced by explosive volcanic activity (e.g., Head et al., 2008). However, as the ESA/JAXA BepiColombo spacecraft is approaching Mercury (Benkhoff et al., 2021), understanding the specific geological and environmental factors influencing the formation and distribution of hollows remains a key research objective (Rothery et al., 2020).

To improve our grasp on this topic, we herein renew the previous hollows data set provided by Thomas et al. (2014a) by updating the database and its degree of detail. In this work we make use of MESSENGER end of mission mosaic data sets (Denevi et al., 2018) to exploit the most up to date data that were not yet available at the time when the previous database was released, particularly the full global mosaics with opposite illumination conditions (e.g., low incidence, East- and West-illumination; Denevi et al., 2018). Instead of focusing solely on their intrinsic morphology or composition, this study aims to elucidate the global stratigraphic distribution of hollows using a statistical approach, laying the groundwork for future multidisciplinary research. We offer GIS-ready polygonal features that delineate hollow fields and provide a quantitative analysis of their surface occurrence. We also provide statistical information on the craters hosting hollows and compare them to the global crater database (Kinczyk et al., 2020). Since most of the population of hollows is contained within impact craters, which excavate the crust of the planet and expose the underlying stratigraphy, it is possible to investigate whether relationships exist between the presence of hollows and specific crater populations, which in turn constrains whether there are one or more identifiable sources. Specifically, to test these hypotheses, we compared the population of craters containing hollows and the global population of craters on Mercury (Kinczyk et al., 2020). This database, hereafter referred to as the global population, is based on a thorough mapping effort that provided a very broad and nearly global coverage of all Mercury craters by classifying them into five morphological classes. Although only craters with diameters larger than 40 km are included, it represents one of the most recent and complete data sets available. By comparing diameter, depth, and degradation between the two crater data sets, it is possible to reveal differences between the global crater population and the subpopulation of hollow containing craters. This helps to understand whether the hollow containing craters are a random subset of the global population, and thus closely replicates its main characteristics or not.

2. Methods

Our analysis relied on image and topographic data provided by the Mercury Dual Imaging System (MDIS; Hawkins et al., 2007) and the Mercury Laser Altimeter (MLA; Cavanaugh et al., 2007) of MESSENGER. The monochrome moderate solar incidence angle Map Projected Basemap Reduced Data Record (BDR) was used as the primary basemap, which has a resolution of approximately 166 m/pixel and was complemented by the consultation of the Map Projected High-Incidence Angle Basemap Illuminated from the East (HIE), the Map Projected High-Incidence Angle Basemap Illuminated from the West (HIW), and the low-incidence angle mosaic (LOI) at a similar resolution (~166 m/pixel) (Denevi et al., 2018). The analysis also incorporated data from the United States Geological Survey (USGS) stereo-derived Digital Elevation Model (DEM) at ~655 m/pixel (Becker et al., 2016) and, where available, MLA-derived DEMs. Observations of the global mosaics and accompanying DEMs, mapping, and measurements were performed using QGIS software (https://qgis.org/).

Hollow identification was based on both morphology and reflectance, while also considering the terrains and setting in which they were found. We used geomorphological characteristics to perform a global search and mapping of hollows across the Mercury surface (e.g., De Toffoli et al., 2021) starting from the revision of all the previously identified hollow locations (Thomas et al., 2014a). Features were interpreted as hollows when they appeared as irregularly shaped depressions with predominantly smooth edges and dimensions spanning between hundreds of meters to several kilometers wide. These shallow, rimless features often exhibit high-reflectance interiors and diffuse bright halos. The absence of a rim, along with a flat floor and a halo, the smooth, flat interior, occasionally featuring small bumps or mesas interpreted as remnants of the original terrain, distinguishes hollows from small impact craters, pits, vents, or other depressions (Blewett et al., 2011). Hollows generally occur clustered in groups (hollow fields), although isolated instances exist. In some cases the identification of hollows occurred under conditions close to the resolution limit or where limitations existed due to feature illumination or visibility, for all these instances it was reported that a degree of uncertainty existed (Table 1). The upcoming BepiColombo mission will use higher resolution cameras to finally overcome these observational challenges (Rothery et al., 2020).

Table 1
Complete List of Key Traits Including Descriptions and Brief Identification Code Used for Data Tabulation

Trait	Description	Code
Global Location		
Located on the North Polar Region	above 60° latitude	N_Pole
Located on the Northern Hemisphere	between 0° and 60° latitude	N_Hemi
Located on the Southern Hemisphere	between 0° and −60° latitude	S_Hemi
Located on the South Polar Region	below −60° latitude	S_Pole
Located on the Hot Pole 0°	0° ± 60° longitudinal range	HP0
Located on the Hot Pole 180°	180° ± 60° longitudinal range	HP180
Local Position		
Located on Plains		Plains
Located within Crater		Crater
Located on Crater Floor		C_Floor
Located on Crater Peak		C_Peak
Located on Crater Ejecta		C_Ejecta
Located on Crater Walls, Rims, and Rings		C_Walls
Located within Crater with Infill		Infill
Relation to Other Proximal Features		
Located on LRM - Color Enhanced Map	blue pixels from color enhanced MDIS global mosaic (Denevi et al., 2018)	LRM_blue
Located on LRM - Klima et al., 2018	LRM defined pixels according to Klima et al. (2018)	LRM_Klima
Located close to Vents	<50 km from vents or facula deposits, that is, pyroclastic deposits characterized by a central pit (vent) surrounded by a spectrally bright and red deposit (Galiano et al., 2022; Thomas et al., 2014b)	Pits
Located close to Tectonic Features	<50 km from tectonic features (Man et al., 2023)	Tectonic
Accuracy Limitation		
Putative Hollow	locations where, due to low resolution limits or illumination/location limits, not all key carachteristics appeared well visible	Putative

We improved upon previous global observations by sorting the various locations and settings in which hollow fields were found into a total of 18 different key traits (Table 1). These categories include broad and localized areas, like specific terrains, specific locations within craters, and proximity to other landforms. These were ultimately placed in a boolean matrix where 0 stands for false and 1 stands for true in reference to the presence of each trait for the 476 observed hollow locations. When hollows were included into craters, Δ elevation was calculated from the DEM by computing the difference between minimum and maximum elevation values within each area.

Additional information was collected from available geological maps of Mercury, including the geological units on which the hollows are situated and the units that are in contact with the hollow-bearing craters. However, since several areas of Mercury remain unmapped, this analysis was limited to hollows in regions with existing geological maps, that is, quadrangles H02 (Galluzzi et al., 2016), H03 (Guzzetta et al., 2017), H04 (Mancinelli et al., 2016), H05 (Wright et al., 2019), H06 (Giacomini et al., 2022), H07 (King & Scott, 1990), H10 (Malliband et al., 2023), H11 (Trask & Dzurisin, 1984), H12 (Spudis & Prosser, 1984), H13 (Man et al., 2023), H-14 (Pegg et al., 2021).

Making use of the data gathered in the compiled boolean matrix, further analyses were performed to determine the abundance of key trait occurrences in the global population and in population subgroups, as described by Equations 1 and 2. Each subgroup corresponds to the family of hollow fields that display individual features among those listed in Table 1.

$$P(A) = \frac{N_a}{N} \quad (1)$$

Equation 1 describes the probability of the occurrence of condition A (i.e., one of the key traits given above) *P(A)* by computing the ratio between the total number of hollow fields exhibiting the given condition A (N_a) and the total number of detected hollow fields *N*. When we instead investigate the probability of the occurrence of condition A within subgroups of hollow fields, we needed to link the probability of the occurrence of condition A to the occurrence of condition B, that represents the key trait through which we selected the elements belonging to the examined subgroup. This relationship is described by Equation 2:

$$P(A|B) = \frac{P(A \cap B)}{P(B)} = \frac{N_{ab}}{N_b} \quad (2)$$

where *P(A|B)* is the probability of the occurrence of condition A in a subgroup of hollow fields characterized by the display of condition B, *P(A∩B)* is the probability of the contextual occurrence of condition A and B, *P(B)* is the probability of the occurrence of condition B, and N_{ab} is the number of hollow fields that both display condition A and B. Finally, we also determined the extent to which each subgroup differs from the overall population calculating a dependency index *I* that estimates the relationship between the respective probabilities of conditions occurrence (Equation 3):

$$I\,(A|B) = \frac{P(A|B)}{P(A)} \quad (3)$$

3. Results

The previous catalog of hollows compiled by Thomas et al. (2014a) counted 445 locations where hollows were identified. We reviewed their list and compiled an updated list of 476 locations (Figure 1), among which 41 are new. Accordingly, 10 areas that were interpreted to be hollow-bearing by Thomas et al. (2014a) have been discarded due to lack of evidence.

Global trends (Table 2) show that hollows appear to be predominantly located in the northern hemisphere of Mercury. However, due to MESSENGER's highly elongated and eccentric orbit, images of the southern hemisphere have lower spatial resolution compared to those of the northern hemisphere possibly leading to identification biases. In good accordance with previous observations, we also detected that 77% of hollow-bearing locations are within ±60° (Thomas et al., 2014a) of the "hot poles" (0°E and 180°E; Melosh & McKinnon, 1988; Bauch et al., 2021). Similarly, we observed that nearly 90% of hollows locations are associated with craters and/or their ejecta. We find that hollows can be localized in one single portion of the crater or dispersed over larger areas. For instance, when hollows are observed on crater ejecta, they tend to extend toward the crater and be present on the rim as well. When hollows are associated with craters: 51% of them are found on the crater floor, 34% of them are found on the central peak, 57% are found on crater walls, rims or rings, and 18% of them are found on crater ejecta. Complementary to that, hollows located on Mercury's plains, that is, displaying no evidence of spatial connection with an impact crater, are significantly less (11% of hollow-bearing locations) and consequently there is a possibility of weaker and less meaningful statistics in estimating the occurrence of additional conditions associated with hollows on plains. Finally, we herein present a quantitative correlation between hollows and LRM, whereas previously hollows have been only qualitatively associated with LRM (Blewett et al., 2018; Thomas et al., 2014a). We observe that 75% of hollow locations are on LRM of the enhanced color map, that is, areas characterized by materials with low reflectance relative to the Mercurian average (Blewett et al., 2013; Denevi et al., 2009; Xiao et al., 2013), in agreement with earlier publications (e.g., Thomas et al., 2014a). The percentage of hollow-bearing locations on LRM drops to 50% when using LRM classification as defined by Klima et al. (2018), along with a reduction of LRM areas. Thus, the relationship between hollows and LRM depends strongly on the given definition of each compositional unit since substantial variations are observed among different studies. Overall, LRM can be spatially associated with hollows although they are not necessarily genetically linked (Barraud et al., 2020, 2023).

10.1029/2024EA003854

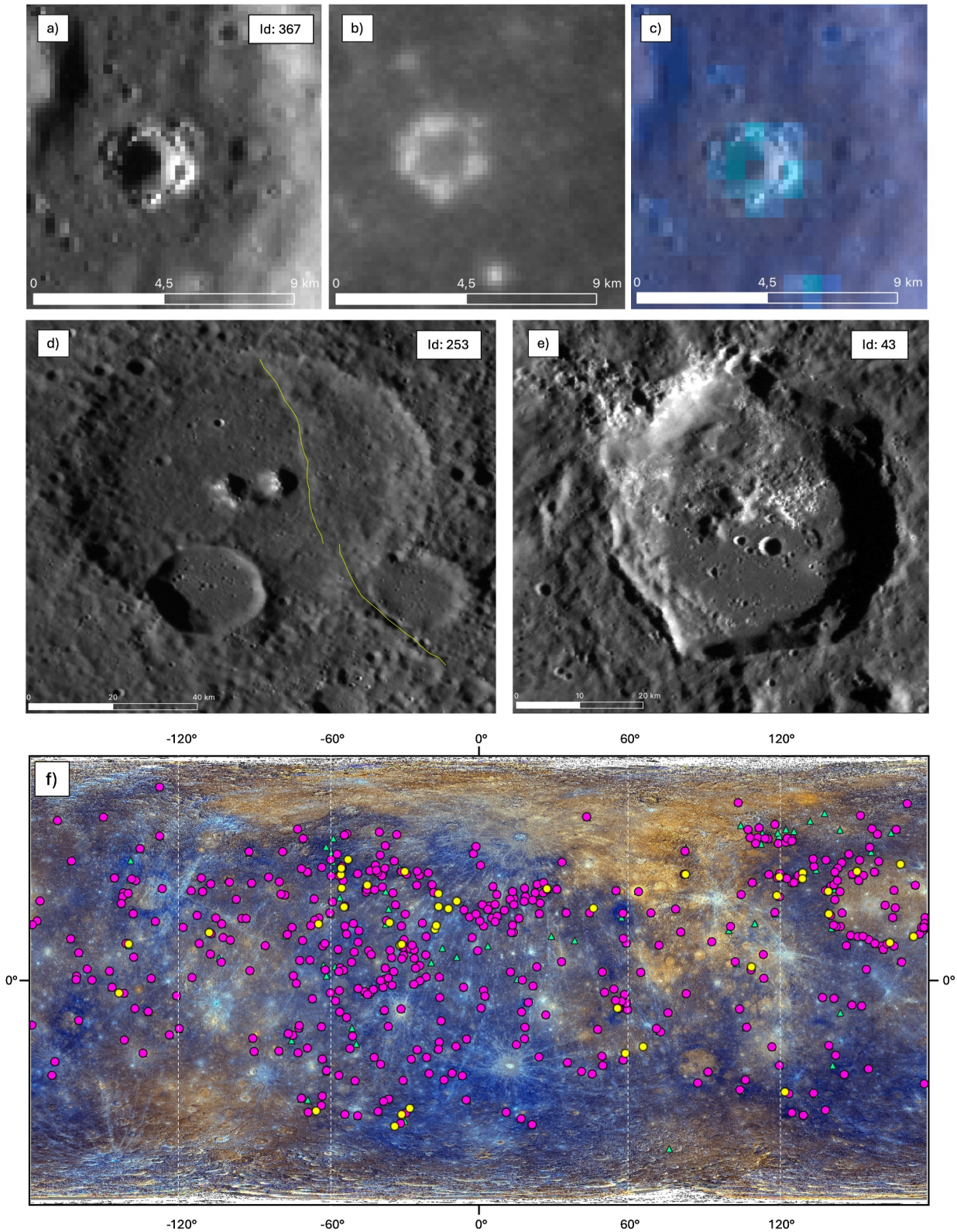

Figure 1. Instances of mapped hollows: (a) hollows in one of the smallest hollow-bearing craters observed on the BDS mosaic, (b) LOI mosaic, and (c) Enhanced Color mosaic; (d) hollows on crater peak closeby tectonic structures (Man et al., 2023); (e) hollows on crater floor. (f) Global overview of hollows' locations: pink dots indicate hollows reported in Thomas et al. (2014a) that have been confirmed in this updated database; yellow dots mark newly identified hollows; green triangles represent hollows from the Thomas et al. (2014a) database that have either not been confirmed or have been spatially adjusted.

Table 2

A Visualization of the Presence of Hollows in Relation to the Key Traits (Table 1)

a)

	N Pole	N Hemi	S Hemi	S Pole	Plains	Crater	C_Floor	C_Peak	C_Ejecta	LRM_blue	LRM_Klima	Pits	Tectonics	C_Walls	HP 180	HP 0	Infill	Putative	N°elements
TOT	0.03	0.68	0.30	0.00	0.11	0.89	0.51	0.34	0.18	0.75	0.40	0.12	0.26	0.57	0.29	0.48	0.19	0.58	476
N Pole	1.00	0.00	0.00	0.00	0.15	0.85	0.38	0.38	0.31	0.62	0.23	0.00	0.15	0.54	0.62	0.15	0.15	0.69	13
N Hemi	0.00	1.00	0.00	0.00	0.14	0.86	0.49	0.33	0.15	0.69	0.34	0.09	0.26	0.57	0.31	0.46	0.15	0.58	322
S Hemi	0.00	0.00	1.00	0.00	0.04	0.96	0.57	0.35	0.26	0.92	0.55	0.19	0.27	0.60	0.21	0.57	0.28	0.57	141
Plains	0.04	0.85	0.11	0.00	1.00	0.00	0.00	0.00	0.00	0.64	0.36	0.11	0.45	0.00	0.66	0.15	0.00	0.81	53
Crater	0.03	0.65	0.32	0.00	0.00	1.00	0.57	0.38	0.21	0.77	0.41	0.12	0.23	0.65	0.25	0.53	0.21	0.55	423
C_Floor	0.02	0.65	0.33	0.00	0.00	1.00	1.00	0.46	0.19	0.77	0.37	0.16	0.21	0.54	0.24	0.52	0.25	0.39	243
C_Peak	0.03	0.66	0.31	0.00	0.00	1.00	0.89	1.00	0.19	0.72	0.36	0.07	0.12	0.52	0.25	0.47	0.23	0.40	162
C_Ejecta	0.05	0.55	0.41	0.00	0.01	0.99	0.52	0.34	1.00	0.78	0.49	0.11	0.25	0.91	0.27	0.49	0.14	0.52	88
LRM_blue	0.02	0.62	0.36	0.00	0.09	0.91	0.52	0.33	0.19	1.00	0.51	0.10	0.25	0.60	0.27	0.52	0.17	0.57	360
LRM_Klima	0.02	0.58	0.41	0.00	0.10	0.90	0.47	0.31	0.23	0.96	1.00	0.09	0.27	0.68	0.32	0.50	0.16	0.61	191
Pits	0.00	0.51	0.49	0.00	0.11	0.89	0.71	0.22	0.18	0.64	0.31	1.00	0.35	0.55	0.24	0.51	0.35	0.40	55
Tectonics	0.02	0.67	0.31	0.00	0.20	0.80	0.41	0.16	0.18	0.74	0.42	0.15	1.00	0.47	0.25	0.51	0.28	0.65	123
C_Walls	0.03	0.67	0.31	0.00	0.00	1.00	0.48	0.31	0.29	0.79	0.47	0.11	0.21	1.00	0.26	0.53	0.15	0.58	274
HP 180	0.06	0.73	0.22	0.00	0.25	0.75	0.42	0.29	0.17	0.70	0.45	0.09	0.22	0.52	1.00	0.00	0.18	0.58	139
HP 0	0.01	0.64	0.35	0.00	0.03	0.97	0.55	0.33	0.19	0.81	0.41	0.12	0.27	0.63	0.00	1.00	0.15	0.58	231
Infill	0.02	0.54	0.44	0.00	0.00	1.00	0.67	0.42	0.13	0.70	0.35	0.21	0.39	0.45	0.28	0.38	1.00	0.38	89
Putative	0.03	0.68	0.29	0.00	0.16	0.84	0.34	0.23	0.17	0.74	0.42	0.08	0.29	0.58	0.29	0.49	0.12	1.00	276

b)

	N Pole	N Hemi	S Hemi	S Pole	Plains	Crater	C_Floor	C_Peak	C_Ejecta	LRM_blue	LRM_Klima	Pits	Tectonics	C_Walls	HP 180	HP 0	Infill	Putative
N Pole		0.00	0.00		1.38	0.95	0.75	1.13	1.67	0.82	0.58	0.00	0.60	0.94	2.11	0.32	0.82	1.20
N Hemi	0.00		0.00		1.26	0.97	0.96	0.98	0.81	0.91	0.85	0.75	1.00	0.99	1.08	0.95	0.80	1.00
S Hemi	0.00	0.00			0.38	1.08	1.13	1.04	1.38	1.22	1.38	1.66	1.05	1.04	0.73	1.19	1.48	0.98
Plains	1.38	1.26	0.38			0.00	0.00	0.00	0.10	0.85	0.90	0.98	1.76	0.00	2.27	0.31	0.00	1.40
Crater	0.95	0.97	1.08		0.00		1.13	1.13	1.11	1.02	1.02	1.00	0.91	1.13	0.84	1.09	1.13	0.95
C_Floor	0.75	0.96	1.13		0.00	1.13		1.34	1.03	1.01	0.91	1.39	0.81	0.95	0.82	1.08	1.32	0.68
C_Peak	1.13	0.98	1.04		0.00	1.13	1.34		1.00	0.96	0.91	0.64	0.48	0.90	0.85	0.97	1.22	0.68
C_Ejecta	1.67	0.81	1.38		0.10	1.11	1.03	1.00		1.04	1.22	0.99	0.97	1.58	0.94	1.01	0.73	0.90
LRM_blue	0.82	0.91	1.22	n/a	0.85	1.02	1.01	0.96	1.04		1.28	0.84	0.98	1.05	0.92	1.07	0.92	0.98
LRM_Klima	0.58	0.85	1.38		0.90	1.02	0.91	0.91	1.22	1.28		0.77	1.06	1.18	1.11	1.03	0.87	1.05
Pits	0.00	0.75	1.66		0.98	1.00	1.39	0.64	0.99	0.84	0.77		1.34	0.95	0.81	1.05	1.85	0.69
Tectonics	0.60	1.00	1.05		1.76	0.91	0.81	0.48	0.97	0.98	1.06	1.34		0.82	0.86	1.06	1.53	1.12
C_Walls	0.94	0.99	1.04		0.00	1.13	0.95	0.90	1.58	1.05	1.18	0.95	0.82		0.90	1.09	0.78	1.01
HP 180	2.11	1.08	0.73		2.27	0.84	0.82	0.85	0.94	0.92	1.11	0.81	0.86	0.90		0.00	0.96	1.01
HP 0	0.32	0.95	1.19		0.31	1.09	1.08	0.97	1.01	1.07	1.03	1.05	1.06	1.09	0.00		0.79	1.01
Infill	0.82	0.80	1.48		0.00	1.13	1.32	1.22	0.73	0.92	0.87	1.85	1.53	0.78	0.96	0.79		0.66
Putative	1.20	1.00	0.98		1.40	0.95	0.68	0.68	0.90	0.98	1.05	0.69	1.12	1.01	1.01	1.01	0.66	

Note. Complete raw data available in the supplementary materials. In Table (a) probabilities and conditional probabilities are displayed. Values span from 0 (Red) to 1 (Green). In the last column the number of hollow fields included in each investigated group is reported. In Table (b) we calculated dependency index I. When $0 < I < 1$ there is negative correlation between conditions occurrence (0 = brown; 1 = white), when $I > 1$ there is positive correlation between conditions occurrence ($I > 1$ = green).

3.1. Hollow-Bearing Craters

The updated global database of hollows allows for an investigation into their stratigraphic occurrence, aiming to constrain their formation. By comparing the characteristics of craters containing hollows (i.e., diameter, depth, and degradation state) with the broader global crater population on Mercury, it becomes feasible to discern whether hollow-bearing craters represent a random subset of the global population or exhibit distinct characteristics.

Several differences are detectable between these two crater groups. Indeed, even though the global population does not include craters smaller than 40 km, we note that the population of hollow-bearing craters increases more slowly as diameter decreases, compared to the global population (Figure 2b). The relationship between diameters and present crater depths (Δ elevation) in hollow-bearing craters differs distinctly from the global population. Δ elevation shows a notable divergence in craters with Δ elevation less than approximately 1,500 m. Below this threshold, hollow-bearing craters are exclusively small in diameter (<50 km) while larger diameter craters are present in the global population (Figure 2c). Despite this, hollow-bearing craters cover an overall Δ elevation range identical to that of the global population. We additionally investigated the *diameter* versus *Δ elevation* distribution of subgroups of the hollow-bearing crater population depending on other hollows traits (Table 1), but no noticeable deviations from the distribution of the main group were found.

Since about one-third of the craters with hollows are included in a global study of morphological crater degradation on Mercury (Kinczyk et al., 2020), we can compare the preservation state of these craters with the global population. In Kinczyk et al. (2020), degradation classes range from 5, the freshest (DC5), to 1, the most degraded (DC1). Globally, there is an abundance of very degraded craters reaching very large diameters that gradually decreases in abundance and diameter (Figures 2d and 2e). For the hollow-bearing craters, the fresh groups of DC4 and DC5 show a trend similar to the global one, while a marked countertrend is evident for DC1, DC2, and DC3.

We carried out further analyses by computing the dependency index to also study the joint occurrence of hollows key traits, degradation classes and geological units (both taking into account the crater unit and the contact units;

10.1029/2024EA003854

Figure 2. (a) Distribution of absolute elevation of the whole hollow population. (b) Crater abundance (bins = 100 km) divided by crater diameter is represented for both the population of hollow-bearing craters (green; tot: 438) and the global population of craters (purple; tot: 3,253, including hollow-bearing craters with $D < 40$). Since craters smaller than 40 km in diameter are not mapped in the global data set, all $D < 40$ km hollow-bearing craters have been grouped into a separate bin (tot: 226). (c) Plot of diameters against the Δ elevation for both populations. Goodness of mapping (GoM) was tested by applying a 10 km buffer around the manually mapped polygon limit to search for the largest maximum in the rim area (yellow circles). No significant change is observed from the result of manual mapping (green diamonds). Crater degradation frequency (d) and distribution against diameter (e) for both hollow-bearing craters and the global population (global data extend off the plot for heavy degraded classes DC1 and DC2).

e.g. Galluzzi et al., 2016). The only significant relationship we identified, that thus deviates from the general trend, is an overall tendency to find deeply seated tectonic structures and volcanic vents more frequently in hollow-bearing craters that are degraded (or mapped as older craters) than in fresher and more pristine craters (see in Supporting Information S1). For example, we observe that, overall, 10% of hollow-bearing craters are

associated with volcanic pits and 20% with tectonic structures. However, when focusing on DC2 hollow-bearing craters, these values increase to 19% for pits and 48% for tectonic structures. This trend becomes progressively less pronounced in fresher craters, and by DC5, the associations with pits return to the same levels observed in the overall hollow-bearing crater population, while the association with tectonic structures even reverses. It is important to note that this is not a biunivocal relationship. Although in the hollow-bearing crater population we observe more vents and structures in degraded craters than in fresh craters, this does not imply that pits and faults are generally exclusive to degraded craters. This trend is evident from the analysis of the dependency index, comparing the occurrence of faults and vents in craters with hollows to their occurrence within specific crater subgroups categorized by degradation class and geological unit.

4. Discussion

Hollows are a planet-wide feature observed across the surface of Mercury. Their occurrence seems to be ubiquitous, however their distribution has the tendency to favor specific surface morphologies and geologic settings, foremost among them impact craters. Impact events play a fundamental role in opening a window into Mercury's subsurface, as they excavate and expose otherwise buried materials. Thus, studying how hollows appear distributed and correlated with the crater population represents an opportunity to assess the stratigraphic significance of hollows and reveal certain aspects of their origin. Furthermore, by comparing the specific structures and morphologies within craters (i.e., tectonic and volcanic) that hollows favor, we can better constrain how buried volatiles might be reaching the surface presently.

One of the main questions related to the origin of hollows is whether a single source volatile bearing layer exists (e.g., Blewett et al., 2011). The observations reported in this paper rule out this hypothesis. Consequently, it is not possible to trace the formation of these morphologies to one or more specific stratigraphic or elevational levels. Indeed the various locations of hollows align with the global range of crater excavation as no cut-offs are detectable at specific depth of excavation (Figure 2b) or elevation (Figure 2a), suggesting a lack of evidence for a singular planet-wide unit associated with volatile materials driving their formation. We thus argue for a distributed presence of volatile bearing materials within the crust, which might be non-homogeneous horizontally across the entire planet, but appears to be vertically ubiquitous in the upper few kilometers of the crust. Therefore, volatiles may not be evenly spread across the planet's surface, but appear to be consistently present at various crustal depths. The lack of a clear correlation between hollow occurrence and specific geological units further underscores the notion that these features are not linked to a single, widespread source of volatile materials. In accordance with this observation, our inference also leans toward the likelihood of endogenous volatiles contributing to the formation of hollows. This inference is drawn from the observed pattern where smaller craters do not exhibit a higher abundance of hollows compared to the global population. Although the available global data set of craters on Mercury lacks information for craters smaller than 40 km leaving some uncertainties, the abundance of craters at the available diameters in the global population compared to the known abundance distribution of hollow-bearing craters (including those smaller than 40 km), makes it unlikely that small craters are overrepresented in the hollow-bearing crater population. If volatiles were brought to the surface by impactors, we would expect to see hollows more frequently within craters where the survival chances of impactor's materials are higher, typically smaller and less energetic impacts. However, the lack of such a trend suggests an interplay of factors influencing the distribution of volatiles more strictly linked to endogenous, rather than exogenous, drivers.

We also suggest that hollows are outcomes of processes reworking pre-existing materials. They occur preferentially in either fresher (i.e., younger) craters or in highly degraded (i.e., older) craters exhibiting subsequent tectonic/volcanic activity, where volatile-rich materials have the opportunity to be brought closer to the surface by earlier impacts through excavation, fracturing/faulting, and lava infilling, occurring both singularly and collectively. This reworking of material increases the likelihood of exposure of otherwise buried materials to the surface, or shallow subsurface. This also suggests that hollows are likely short-lived. Indeed the fact that hollows occur infrequently in old craters, and when they do, are more frequently associated with tectonic or volcanic structures, suggests that hollows have an overall low preservation potential, at least compared to other surface morphologies found on Mercury (e.g., volcanic vents, Thomas et al., 2014b). Also supporting this hypothesis is the gap between the population of hollow-bearing craters and the overall population of craters (Figure 2b) for shallow crater depths (<1,500 m). The larger craters in this range, missing in the hollow-bearing population, may represent older impact morphologies that degraded over time or were flooded by subsequent lava flows. This evidence does not exclude the possibility that hollows have been forming on Mercury's surface since very ancient

geological epochs, it indicates instead that their preservation potential is low, making them ephemeral. Their short life span might possibly be further exacerbated by their shallow morphology that likely allows for a faster degradation. Given that morphological degradation begins immediately after the hollow-formation process concludes, the formation phase is likely shorter than the overall lifespan of hollows morphology. Hence, the volatile escape is likely ephemeral.

5. Conclusions

In conclusion, the stratigraphical occurrence of hollows and their spatial association to other geological features reveals the intricate nature of their formation processes that cannot yet be attributed to a definitive set of conditions or mechanisms, indicating that further investigation is needed to pinpoint the specific combination of responsible factors. The dynamic nature of hollows, with their occurrence in association with both impact and volcano-tectonic events, hints at a complex history of material redistribution on the planet's surface. Overall we herein discuss evidence supporting.

- the lack of a single (or a limited and measurable number) planet-wide unit bearing the volatile materials necessary for hollows formation due to: (a) the wide range of elevations and excavation depths at which hollows are found, indicating their presence throughout all exposed crustal levels; (b) lack of correlation between hollows and any geological units.
- the short-lived nature of hollows due to: (a) a relevant lack of hollows in degraded craters compared to younger fresher craters; (b) a higher abundance of hollows in degraded craters also containing structures or vents.

Data Availability Statement

Base maps used in this work are available from the PDS Geosciences Node (https://ode.rsl.wustl.edu/mercury/datasets). For mapping and measurements the QGIS software was used, which is free and open source (https://www.qgis.org/en/site/index.html). The tabulated raw data produced in this paper are provided as supplementary information. In addition to the tables, we also provided the GIS-ready shapefile containing all the polygons inscribing the areas where the hollows were observed. Zenodo link: https://zenodo.org/records/14000558. Zenodo doi: https://doi.org/10.5281/zenodo.14000558.

Acknowledgments
We acknowledge funding from the Italian Space Agency (ASI) under ASI-INAF agreement 2017-47-H.0. The authors gratefully acknowledge Susan Conway and David T. Blewett for the helpful and constructive revisions.

References

Barraud, O., Doressoundiram, A., Besse, S., & Sunshine, J. M. (2020). Near-ultraviolet to near-infrared spectral properties of hollows on Mercury: Implications for origin and formation process. *Journal of Geophysical Research: Planets*, *125*(12), e2020JE006497. https://doi.org/10.1029/2020JE006497

Barraud, O. A., Besse, S. B., & Doressoundiram, A. (2023). Low sulfide concentration in Mercury's smooth plains inhibits hollows. *Science Advances*, *9*(12), eadd6452. https://doi.org/10.1126/sciadv.add6452

Bauch, K. E., Hiesinger, H., Greenhagen, B. T., & Helbert, J. (2021). Estimation of surface temperatures on Mercury in preparation of the MERTIS experiment onboard BepiColombo. *Icarus*, *354*, 114083. https://doi.org/10.1016/j.icarus.2020.114083

Becker, K. J., Robinson, M. S., Becker, T. L., Weller, L. A., Edmundson, K. L., Neumann, G. A., et al. (2016). First global digital elevation Model of Mercury. *Lunar and Planetary Science Conference*, *47*, 2959.

Benkhoff, J., Murakami, G., Baumjohann, W., Besse, S., Bunce, E., Casale, M., et al. (2021). BepiColombo-mission overview and science goals. *Space Science Reviews*, *217*(8), 90. https://doi.org/10.1007/s11214-021-00861-4

Blewett, D. T., Chabot, N. L., Denevi, B. W., Ernst, C. M., Head, J. W., Izenberg, N. R., et al. (2011). Hollows on Mercury: MESSENGER evidence for geologically recent volatile-related activity. *Science*, *333*, 1856–1859.

Blewett, D. T., Ernst, C. M., Murchie, S. L., & Vilas, F. (2018). Mercury's hollows. In L. Nittler & B. Anderson (Eds.), *Mercury: The view after MESSENGER* (pp. 324–345). Cambridge Univ. Press.

Blewett, D. T., Vaughan, W. M., Xiao, Z., Chabot, N. L., Denevi, B. W., Ernst, C. M., et al. (2013). Mercury's hollows: Constraints on formation and composition from analysis of geological setting and spectral reflectance. *Journal of Geophysical Research: Planets*, *118*(5), 1013–1032. https://doi.org/10.1029/2012je004174

Cavanaugh, J. F., Smith, J. C., Sun, X., Bartels, A. E., Ramos-Izquierdo, L., Krebs, D. J., et al. (2007). The Mercury laser altimeter instrument for the MESSENGER mission. *Space Science Reviews*, *131*(1), 451–479. https://doi.org/10.1007/978-0-387-77214-1_13

Denevi, B. W., Chabot, N. L., Murchie, S. L., Becker, K. J., Blewett, D. T., Domingue, D. L., et al. (2018). Calibration, projection, and final image products of MESSENGER's mercury dual imaging system. *Space Science Reviews*, *214*(1), 2. https://doi.org/10.1007/s11214-017-0440-y

Denevi, B. W., Robinson, M. S., Solomon, S. C., Murchie, S. L., Blewett, D. T., Domingue, D. L., et al. (2009). The evolution of Mercury's crust: A global perspective from MESSENGER. *Science*, *324*(5927), 613–618. https://doi.org/10.1126/science.1172226

De Toffoli, B. (2024). Hollows on Mercury: A comprehensive analysis of spatial patterns and their relationship to craters and structures [Dataset]. *Earth and Space Science. Zenodo*. https://doi.org/10.5281/zenodo.14000558

De Toffoli, B., Plesa, A.-C., Hauber, E., & Breuer, D. (2021). Delta deposits on Mars: A global perspective. *Geophysical Research Letters*, *48*(17), e2021GL094271. https://doi.org/10.1029/2021GL094271

Galiano, A., Capaccioni, F., Filacchione, G., & Carli, C. (2022). Spectral identification of pyroclastic deposits on Mercury with MASCS/MESSENGER data. *Icarus*, *388*, 115233. https://doi.org/10.1016/j.icarus.2022.115233

Galluzzi, V., Guzzetta, L., Ferranti, L., Di Achille, G., Rothery, D. A., & Palumbo, P. (2016). Geology of the Victoria quadrangle (H02), Mercury. *Journal of Maps*, *12*(sup1), 227–238. https://doi.org/10.1080/17445647.2016.1193777

Giacomini, L., Galluzzi, V., Massironi, M., Ferranti, L., & Palumbo, P. (2022). Geology of the Kuiper quadrangle (H06), Mercury. *Journal of Maps*, *18*(2), 246–257. https://doi.org/10.1080/17445647.2022.2035268

Guzzetta, L., Galluzzi, V., Ferranti, L., & Palumbo, P. (2017). Geology of the Shakespeare quadrangle (H03), Mercury. *Journal of Maps*, *13*(2), 227–238. https://doi.org/10.1080/17445647.2017.1290556

Hawkins, S. E., Boldt, J. D., Darlington, E. H., Espiritu, R., Gold, R. E., Gotwols, B., et al. (2007). The Mercury dual imaging system on the MESSENGER spacecraft. *Space Science Reviews*, *131*(1–4), 247–338. https://doi.org/10.1007/s11214-007-9266-3

Head, J. W., Murchie, S. L., Prockter, L. M., Robinson, M. S., Solomon, S. C., Strom, R. G., et al. (2008). Volcanism on Mercury: Evidence from the first MESSENGER flyby. *Science*, *321*(5885), 69–72. https://doi.org/10.1126/science.1159256

Kinczyk, M. J., Prockter, L. M., Byrne, P. K., Susorney, H. C. M., & Chapman, C. R. (2020). A morphological evaluation of crater degradation on Mercury: Revisiting crater classification with MESSENGER data. *Icarus*, *341*, 113637. https://doi.org/10.1016/j.icarus.2020.113637

King, J. S., & Scott, D. H. (1990). *Geologic map of the Beethoven quadrangle of Mercury. Map I-2048 (H-7)*. Misc. Investigations Ser. U.S. Geologic Survey.

Klima, R. L., Denevi, B. W., Ernst, C. M., Murchie, S. L., & Peplowski, P. N. (2018). Global distribution and spectral properties of low-reflectance material on Mercury. *Geophysical Research Letters*, *45*(7), 2945–2953. https://doi.org/10.1002/2018GL077544

Man, B., Rothery, D. A., Balme, M. R., Conway, S. J., & Wright, J. (2023). Widespread small grabens consistent with recent tectonism on Mercury. *Nature Geoscience*, *16*(10), 856–862. https://doi.org/10.1038/s41561-023-01281-5

Mancinelli, P., Minelli, F., Pauselli, C., & Federico, C. (2016). Geology of the Raditladi quadrangle, Mercury (H04). *Journal of Maps*, *12*(sup1), 190–202. https://doi.org/10.1080/17445647.2016.1191384

Melosh, H. J., & McKinnon, W. B. (1988). *The tectonics of Mercury. Mercury*, F. Vilas, C. R. Chapman, & M. S. Matthews (Eds.). University of Arizona Press.

Murchie, S. L., Klima, R. L., Denevi, B. W., Ernst, C. M., Keller, M. R., Domingue, D. L., et al. (2015). Orbital multispectral mapping of Mercury with the MESSENGER Mercury Dual Imaging System: Evidence for theorigins of plains units and low-reflectance material. *Icarus*, *254*, 287–305. https://doi.org/10.1016/j.icarus.2015.03.027

Pegg, D. L., Rothery, D. A., Balme, M. R., Conway, S. J., Malliband, C. C., & Man, B. (2021). Geology of the Debussy quadrangle (H14), Mercury. *Journal of Maps*, *17*(2), 718–729. https://doi.org/10.1080/17445647.2021.1996478

Rothery, D. A., Massironi, M., Alemanno, G., Barraud, O., Besse, S., Bott, N., et al. (2020). Rationale for BepiColombo studies of Mercury's surface and composition. *Space Science Reviews*, *216*(4), 1–46. https://doi.org/10.1007/s11214-020-00694-7

Solomon, S. C., McNutt, R. L., Jr., Gold, R. E., & Domingue, D. L. (2007). MESSENGER mission overview. *Space Science Reviews*, *131*(1-4), 3–39. https://doi.org/10.1007/s11214-007-9247-6

Spudis, P. D., & Prosser, J. G. (1984). *Geologic map of the michelangelo quadrangle of Mercury, map I-1659, Misc. Investigations ser*. U. S. Geological Survey.

Thomas, R. J., Rothery, D. A., Conway, S. J., & Anand, M. (2014a). Hollows on Mercury: Materials and mechanisms involved in their formation. *Icarus*, *229*, 221–235. https://doi.org/10.1016/j.icarus.2013.11.018

Thomas, R. J., Rothery, D. A., Conway, S. J., & Anand, M. (2014b). Long-lived explosive volcanism on Mercury. *Geophysical Research Letters*, *41*(17), 6084–6092. https://doi.org/10.1002/2014gl061224

Trask, N. J., & Dzurisin, D. (1984). Geologic map of the discovery (H-11) quadrangle of Mercury. *USGS Misc. Investig. Ser. Map I–1658*.

Wright, J., Rothery, D. A., Balme, M. R., & Conway, S. J. (2019). Geology of the Hokusai quadrangle (H05), Mercury. *Journal of Maps*, *15*(2), 509–520. https://doi.org/10.1080/17445647.2019.1625821

Xiao, Z., Strom, R. G., Blewett, D. T., Byrne, P. K., Solomon, S. C., Murchie, S. L., et al. (2013). Dark spots on Mercury: A distinctive low-reflectance material and its relation to hollows. *Journal of Geophysical Research: Planets*, *118*(9), 1–14. https://doi.org/10.1002/jgre.20115